University of Reading

Wintertime North American weather regimes and the Arctic stratospheric polar vortex

Article

Accepted Version

Lee, S. H., Furtado, J. C. and Charlton-Perez, A. J. ORCID: https://orcid.org/0000-0001-8179-6220 (2020) Wintertime North American weather regimes and the Arctic stratospheric polar vortex. Geophysical Research Letters, 46 (24). pp. 14892-14900. ISSN 0094-8276 doi: 10.1029/2019GL085592 Available at https://centaur.reading.ac.uk/87746/

It is advisable to refer to the publisher's version if you intend to cite from the work. See Guidance on citing.

To link to this article DOI: http://dx.doi.org/10.1029/2019GL085592

Publisher: American Geophysical Union

All outputs in CentAUR are protected by Intellectual Property Rights law, including copyright law. Copyright and IPR is retained by the creators or other copyright holders. Terms and conditions for use of this material are defined in the End User Agreement.

www.reading.ac.uk/centaur

University of Reading

CentAUR

Central Archive at the University of Reading

Reading's research outputs online

Wintertime North American weather regimes and the Arctic stratospheric polar vortex

S. H. Lee[1], J. C. Furtado[2], and A. J. Charlton-Perez[1]

[1]Department of Meteorology, University of Reading, Reading, U.K.
[2]School of Meteorology, University of Oklahoma, Norman, Oklahoma, U.S.A.

Key Points:

- The behavior of three of four regimes over North America is significantly linked to the strength of the lower-stratospheric polar vortex.
- A regime associated with Greenland blocking shows the strongest relationship with the stratospheric polar vortex strength.
- The regime most strongly associated with widespread severe North American cold does not show a dependency on stratospheric vortex strength.

Corresponding author: Simon Lee, s.h.lee@pgr.reading.ac.uk

Abstract

The impact of the Arctic stratospheric polar vortex on persistent weather regimes over North America is so far under-explored. Here we show the relationship between four wintertime North American weather regimes and the stratospheric vortex strength using reanalysis data. We find that the strength of the vortex significantly affects the behavior of the regimes. Whilst a regime associated with Greenland blocking is strongly favored following weak vortex events, it is not the primary regime associated with a widespread, elevated risk of extreme cold in North America. Instead, we find that the regime most strongly associated with widespread extremely cold weather does not show a strong dependency on the strength of the lower-stratospheric zonal-mean zonal winds. We also suggest that stratospheric vortex morphology may be particularly important for cold air outbreaks during this regime.

Plain Language Summary

During winter, the strength of the winds 10-50 km above the Arctic can affect the weather patterns at the surface. Generally, this influence is strongest over the North Atlantic and Europe. However, we show that the strength of stratospheric winds has a significant impact on weather patterns across North America. Our results indicate that knowledge of the stratospheric winds can provide a greater understanding of the evolution of likely weather in this region on longer time periods, including both severely cold weather (and its associated impacts on energy consumption, transport, and human health) or an unusual absence of severe cold.

1 Introduction

The behavior of the stratospheric polar vortex (SPV) is known to influence wintertime tropospheric weather patterns on subseasonal-to-seasonal (S2S) timescales (∼15-60 days ahead) and provide a source of predictability (e.g. Kodera & Chiba, 1995; Kolstad et al., 2010; Sigmond et al., 2013; Tripathi et al., 2015a). The variability of the SPV includes strong vortex events (Tripathi et al., 2015b) and weak vortex events, including major sudden stratospheric warmings (SSWs) (e.g. Charlton & Polvani, 2007). Whilst the mean response to an SSW or weakened SPV is a negative phase of the tropospheric Northern Annular Mode (NAM) and equatorward shift of the eddy-driven jets in the troposphere in the weeks-to-months after (Baldwin & Dunkerton, 2001; Kidston et al., 2015), there is a large amount of case-by-case and regional variability (Karpechko et al., 2017; Kretschmer et al., 2018). Weather regimes provide a helpful framework for examining stratosphere-troposphere coupling. Regimes describe the large-scale atmospheric configuration on any given day and are based on recurrent and persistent patterns in the large-scale circulation (Michelangeli et al., 1995). Because regimes exist on longer timescales than synoptic weather patterns, they provide an opportunity for longer-range prediction, useful for the energy sector (Beerli et al., 2017; Grams et al., 2017) and for the prediction of cold weather extremes in winter (Ferranti et al., 2018). Charlton-Perez et al. (2018) described the influence of the strength of the SPV on weather regimes in the North Atlantic, where the tropospheric response to changes in the stratospheric circulation is typically largest. Using four Atlantic wintertime regimes (following Cassou (2008)), they show the SPV strength significantly affects the occurrence and persistence of each regime, and the transition between regimes. This approach helps illuminate some of the reasons behind different tropospheric responses to stratospheric changes (including, but not limited to, SSWs) in a statistical sense.

Whilst the tropospheric response to changes in the SPV is more variable across North America than in the Euro-Atlantic sector, it has been implicated in driving recent extreme cold weather outbreaks in this region (so-called "polar vortex outbreaks" (Waugh et al., 2017)). These are among recent billion-dollar weather and climate disasters in the

United States (NOAA, 2019). The North American sector is also partly influenced by Atlantic weather patterns and the NAM, which typically respond strongly to changes in the stratosphere. Kretschmer et al. (2018) used cluster analysis in the lower stratosphere to elucidate the influence of the SPV on cold extremes in both North America and Eurasia, finding that a pattern associated with planetary wave reflection was important for anomalous cold over North America. This follows earlier work by Kodera et al. (2016), who found a Pacific blocking response to SSWs dominated by planetary wave reflection, with a downstream trough over North America. In addition, the Pacific sector tropospheric response to stratospheric perturbations is not necessarily of the same sign as in the Euro-Atlantic sector (Ambaum et al., 2001).

Although some prior work has described regimes across North America in a similar sense to the Atlantic regimes (Amini & Straus, 2019; Riddle et al., 2013; Robertson & Ghil, 1999; Straus et al., 2007; Vigaud et al., 2018), the use of regimes is not as common in this region. The number of regimes and the westward and eastward extent of the region used to define the regimes varies between studies, capturing different aspects of Pacific and Atlantic variability. Moreover, the relationship between these regimes and changes in the stratospheric vortex has not yet been quantified.

In this article, we define four tropospheric wintertime regimes across the North American sector and describe the relationship between the regimes and the SPV. We also investigate the link between these regimes and the occurrence of extremely cold weather across North America.

2 Data and Methods

We use 00Z data from the European Centre for Medium-Range Weather Forecasts (ECMWF) ERA-Interim reanalysis (Dee et al., 2011) for all days in December–March in the period January 1979 to December 2017 (a total of 4729 days). December to March is chosen as it encompasses the period of largest SPV variability (e.g. all observed major SSWs have occurred in these months (Butler et al., 2017)). The data are re-gridded to 2.5° horizontal resolution for computational efficiency and since we are considering only large-scale features. We perform an empirical orthogonal function (EOF) decomposition of linearly de-trended 500 hPa geopotential height anomalies (with respect to the daily January 1979–December 2017 climatology) in the sector 180-30°W, 20-80°N (Figure S1). This region is chosen to include the Pacific jet exit region and include relevant North Atlantic variability. De-trending is performed to account for the climate change signal, although it does not notably alter the results (not shown). Data are weighted by the square-root of the cosine of latitude to give equal-area weighting in the covariance matrix. We retain the leading 12 modes of variability, which represent 80% of the total variance in the 500 hPa geopotential height anomaly field. We then perform k-means clustering with k=4 using the Python package *scikit-learn* (Pedregosa et al., 2011). All days are then assigned to a regime based on their minimum Euclidean distance to the cluster centroids; we do not employ "no-regime" days (Grams et al., 2017). The resultant regimes are very similar to those found in Vigaud et al. (2018); they show these regimes are a significant representation based on the classifiability index of Michelangeli et al. (1995), so we do not repeat that calculation here. Our four regimes remain largely unchanged as a subset when five or six clusters are used, further indicating they are dominant patterns and form a concise characterization with reasonably large individual sample sizes.

The probability of regime occurrence (p), which we term the occupation frequency, is given by ratio of the number of days in a given regime (n) to the total number of days (N) in the sample:

$$p = \frac{n}{N} \tag{1}$$

We use 95% confidence intervals with a normal approximation to a binomial proportion confidence interval, given by:

$$p \pm Z\sqrt{\frac{p(1-p)}{N'}} \tag{2}$$

where $Z = 1.96$ from the standard normal distribution. To account for the persistence of the regimes, we employ an effective sample size N', found by using the 1-day persistence probability r_1 (e.g. Wilks, 2011) for each regime in each vortex state,

$$N' = N\frac{1-r_1}{1+r_1} \tag{3}$$

We do not scale N for confidence intervals on the transition probabilities, since these are independent of the preceding regime. We define the strength of the SPV to be the tercile categories of daily zonal-mean zonal wind at 100 hPa and 60°N, following Charlton-Perez et al. (2018). The 100 hPa level is chosen to represent the coupling layer between the stratosphere and troposphere and include only the effects of stratospheric perturbations which propagate into the lower stratosphere. The results are not qualitatively sensitive to the choice of lower-stratospheric level (not shown).

Statistical significance of the composite maps is determined by bootstrap re-sampling with replacement. We construct 95% confidence intervals using 50,000 re-samples per regime over all December to March days in the period 1979–2017. Random days are selected in blocks corresponding to the observed regime 'events', to test the null hypothesis that the composites are the result of random sub-sampling of winter days. Further detail on the bootstrapping method is provided in the Supporting Information.

3 Results

3.1 Circulation regimes

Composites of mean 500 hPa geopotential height anomalies for each of the four regimes are shown in Figure 1. The regimes are very similar to those defined in Straus et al. (2007) (despite a slightly different domain and analysis period) so we follow their naming convention. The least frequent regime (with an occupation frequency of 20%), is the Arctic High (ArH) regime (Figure 1a). It is associated with anomalously high geopotential heights over Greenland and the Canadian archipelago (Greenland blocking), and lower than normal geopotential heights over the Atlantic east of the United States but no significant height anomalies in the Pacific sector. The regime resembles the negative phase of the North Atlantic Oscillation (NAO–), and its occupation frequency is equivalent to the NAO– regime in Charlton-Perez et al. (2018). It is also similar to the tropospheric anomalies associated with cluster 5 in Kretschmer et al. (2018), which they associate with stratospheric planetary wave absorption. The Arctic Low (ArL) regime (Figure 1b) is not a direct counterpart of the ArH regime and is slightly more frequent (25%). Whilst the ArL regime is associated with opposite height anomalies to the ArH regime in the vicinity of Greenland and is somewhat similar to the positive NAO (NAO+), the main signature is a ridge-trough-ridge pattern extending from the Pacific across North America, which resembles the negative phase of the Pacific–North American (PNA–) pattern. The ridge anomaly in the northeast Pacific indicates this regime is associated with a weakened Aleutian low and resembles a negative North Pacific Oscillation (NPO–) (Linkin & Nigam, 2008; Rogers, 1981). The Alaskan Ridge (AkR) regime (Figure 1c), occurring on 26% of days, strongly resembles the Tropical–Northern Hemisphere (TNH) pattern (Mo & Livezey, 1986) and the North American dipole (Wang et al., 2015), the latter of which was linked to the extremely cold North American winter of 2013-14. This regime is also similar to the tropospheric response to cluster 4 in Kretschmer et al. (2018), which they associate with the reflection of planetary waves by the stratosphere. We note that the AkR and ArL regimes are closest to the patterns during "polar vortex outbreaks"

over North America. The most frequent regime (29%) is the Pacific Trough (PT) (Figure 1d), which consists of an anomalous trough centred near Alaska, and an anomalous ridge over continental North America. The trough is consistent with a positive phase of the NPO (NPO+) and the enhancement of the Aleutian Low associated with El Niño, whilst the pattern across North America resembles the positive PNA (PNA+).

3.2 Relationship with the stratosphere

To quantify the relationship between the stratospheric state and each regime, and by considering the long persistence of lower-stratospheric anomalies during winter (Figure S2), we calculate the time-lagged difference in the probability of each regime between weak and strong SPV states. We calculate this difference for the 30 days before and after each day in each regime, conditional on the SPV state at a zero-day lag (day 0) (Figure 2). All but the AkR regime exhibit probability changes greater in magnitude than 0.1, which generally peak around day 0, supporting a stratospheric influence (since this is the given state on which we condition the probability, and we would expect a near-contemporaneous regime response). The ArH regime displays the greatest difference. Its occurrence probability is 0.3–0.4 greater in a contemporaneously weak vortex versus a strong vortex; this difference exceeds 0.1 for all negative lags, which is likely influenced by the long persistence of weak SPV states (and the persistence of this regime in those conditions, c.f. Figure 3b). Moreover, for almost 20 days following a weak SPV, the probability of the ArH regime is more than 0.1 greater than following a strong SPV. Conversely, the probability of the ArL regime is around 0.1 less in the 30 days preceding a weak SPV, but this difference rapidly decays for positive lags. The PT regime becomes 0.1–0.2 less likely following a weak SPV versus a strong SPV for up to 25 days; it does not display a large change in likelihood for negative lags beyond ∼5 days.

Motivated by the preceding analysis, we next compute the probability of each regime given the SPV strength on the preceding day (Figure 3a). Although this is near-instantaneous, it provides a potentially useful framework for extended-range forecasting owing to the persistence and predictability of SPV strength anomalies, and the intrinsic persistence of regimes themselves. The ArH regime demonstrates the largest sensitivity to the stratospheric state, consistent with its negative NAO-like characteristics, with an approximately linear relationship with the tercile SPV strength categories. This regime is seven times more likely following weak SPV states than strong SPV states and is the most likely regime following a weak SPV. The likelihood of the ArL regime increases with increasing SPV strength; it is approximately twice as likely following a strong versus a weak SPV. For the AkR regime, the dependency on the antecedent SPV strength is statistically insignificant. The PT regime is most likely following neutral and strong SPV conditions, and its behavior is generally similar to the ArL regime.

To further understand vortex-dependent changes in the occurrence probabilities, we compute the probability of persisting in a given regime the following day given the SPV strength on the current day (Figure 3b). The persistence of the ArH regime is most strongly dependent on the antecedent SPV strength. Its persistence decreases markedly from 0.86 following a weak SPV to 0.68 following a strong SPV, the lowest persistence probability of any of the regimes for any stratospheric state. This behavior is consistent with its similarity to NAO– (c.f. Figure 3 in Charlton-Perez et al. (2018)). None of the other three regimes exhibit significant changes in persistence probability depending on the SPV strength. Similar results are found when the total duration of each regime is stratified by the SPV strength on the day of transition into the regime (Figure S3), though this metric suggests enhanced duration of the PT regime during strong SPV conditions.

We also consider changes in the transitions between regimes. In Figure 3c we show the probability of transitioning from any other regime into a given regime the following day, given the SPV strength on the current day. Transitioning into the ArH regime is

2.5 times more likely during a weak SPV versus a strong SPV. The opposite is true for the ArL and PT regimes, but the relationship is slightly weaker, with the transitions approximately 50% more likely following a strong SPV versus a weak SPV. We also show the difference in specific regime transitions between a weak and a strong SPV in Table S1, but emphasize that the sample sizes are much smaller for individual transitions (n = 38–90, and even smaller when categorized by SPV strength), making a robust analysis difficult.

In order to discern the association between these regimes and the middle-stratospheric polar vortex (where major SSWs are commonly defined), we show the composite-mean contemporaneous 10 hPa geopotential height anomalies in Figure 4. The pattern during the ArH regime resembles a weak or displaced SPV with an anomalous wavenumber-1 configuration, consisting of anomalously high (low) geopotential heights over the central Arctic (southwest North America and northwest Europe). The anomaly pattern at 10 hPa is similar to that at 500 hPa indicating an equivalent barotropic anomaly structure. The ArL pattern is mostly opposite to ArH, with a strengthened SPV indicated by anomalously low geopotential heights over the central Arctic. The Pacific ridge anomaly present in this regime at 500 hPa does not extend to 10 hPa. The AkR regime features an anomalous wavenumber-2 splitting-type pattern with ridge anomalies in the Atlantic and Pacific, and an anomalous trough over North America. The ridge anomaly over Alaska and trough anomaly over central North America are also present at 500 hPa. The trough anomaly centred near the Hudson Bay is consistent with the similarity of this regime to the "polar vortex" outbreaks driven by a distortion to the vortex. Whilst the AkR regime does not have occurrence, persistence or transition preferences dependent on the antecedent zonal-mean zonal winds, the contemporaneous 10 hPa anomalies indicate significant disruption to the mid-stratospheric vortex. Therefore, this aspect of vortex variability may not be captured in the 100 hPa 60°N zonal-mean zonal wind; instead, the AkR regime may be more influenced by the morphology of the SPV. Additionally, the similarity of this regime to both the response to reflecting major SSWs described in Kodera et al. (2016) and the patterns found during SPV intensification in Limpasuvan et al. (2005) indicates a potential relationship with stratospheric variability. The PT regime is associated with a wavenumber-1 anomaly pattern consisting of a barotropic anomalous ridge over North America and a strengthened SPV.

3.3 Relationship with cold air outbreaks

We next assess the relationship between these regimes and the occurrence of potentially dangerous cold weather outbreaks. To do this, we calculate the probability of severe cold for each regime as the number of days in each regime with normalized 2 m temperature anomalies more than 1.5 standard deviations below the daily mean (similar to the criterion of Thompson & Wallace (2001)). This calculation is performed at each grid-point, and the result is shown in Figure 5. Corresponding maps of composite mean 2 m temperature anomalies for each regime are shown in Figure S4. Despite the large differences between the likelihood, location and extent of cold weather outbreaks in these regimes, we emphasize that all four can bring cold-weather impacts to parts of the Northern Hemisphere.

Whilst the ArH regime (Figure 5a) is the most sensitive to the stratospheric state (c.f. Figures 2 and 3), we find that it is not the most important for widespread wintertime cold weather outbreaks across North America (though there is a significant risk of severe cold (5-10%) for all but northeastern North America during this regime). Moreover, the magnitude of the mean temperature anomalies during this regime are relatively small (Figure S4a). The ArH regime is instead associated with the highest risk (>20%) of severe cold only across northwest Europe, consistent with its NAO– characteristics. We find that severe cold weather outbreaks across the continental interior of North America are most likely during the AkR regime (Figure 5c), with chances of severe cold ex-

ceeding 20%, and mean temperature anomalies widely 5°C below normal (Figure S4c). The ArL regime (Figure 5b) is associated with a 10-15% chance of extreme cold across western North America, including Alaska, whilst in the central and east of the United States there is an absence of extreme cold during this regime. The PT regime (Figure 5d) features an absence of extreme cold across most of North America, with mean temperatures widely more than 5°C above normal (Figure S4d). Extreme cold during this regime is typically confined to western Alaska and the Aleutian Islands, consistent with the western periphery of the anomalous trough. The PT regime also has the lowest overall risk of cold weather outbreaks across the Northern Hemisphere.

4 Summary and Conclusions

In this study we have shown that the behavior of three of four wintertime North American weather regimes is significantly linked to the antecedent strength of the SPV. We find that whilst the ArH regime is most sensitive to the SPV strength, it is not the most important for *widespread* extreme cold outbreaks in North America – particularly in central and northern areas where such extremes correspond to the coldest absolute temperatures. Instead, we find that the AkR regime – which does not display a significant dependence on the lower-stratospheric zonal-mean zonal wind – is associated with the greatest risk of extreme cold across most of North America. Though Figure 4c suggests a possible link exists with the state of the SPV, the similarity of this regime to the TNH pattern suggests that tropical forcing may also exhibit a large control on its behavior (e.g. Hartmann, 2015).

Further work should address the ability of sub-seasonal forecast models to correctly capture the downward coupling of stratospheric anomalies onto these regimes, as well as illuminating the dynamics involved, such as Rossby wave breaking (e.g. Michel & Rivière, 2011), and the impact of model biases. It should also be investigated whether Pacific phenomena on intra-seasonal (such as the Madden-Julian Oscillation (MJO)) to seasonal (e.g. the El Niño-Southern Oscillation (ENSO)) and decadal scales (e.g. the Pacific Decadal Oscillation (PDO)) interact constructively or destructively with the stratospheric influence.

Acknowledgments

S.H.L. was funded by the Natural Environment Research Council (NERC) via the SCENARIO Doctoral Training Partnership (NE/L002566/1). J.C.F. acknowledges funding via the National Science Foundation (NSF) Atmospheric and Geospace Sciences Program (award #AGS-1657905). The ERA-Interim reanalysis dataset is available at https://apps.ecmwf.int/datasets/. We acknowledge two anonymous reviewers for their detailed comments which helped improve the paper.

References

Ambaum, M. H., Hoskins, B. J., & Stephenson, D. B. (2001). Arctic Oscillation or North Atlantic Oscillation? *Journal of Climate*, *14*(16), 3495–3507. doi: 10.1175/1520-0442(2001)014⟨3495:AOONAO⟩2.0.CO;2

Amini, S., & Straus, D. M. (2019). Control of storminess over the Pacific and North America by circulation regimes. *Climate Dynamics*, *52*(7-8), 4749–4770. doi: 10.1007/s00382-018-4409-7

Baldwin, M. P., & Dunkerton, T. J. (2001). Stratospheric harbingers of anomalous weather regimes. *Science*, *294*(5542), 581–584.

Beerli, R., Wernli, H., & Grams, C. M. (2017). Does the lower stratosphere provide predictability for month-ahead wind electricity generation in Europe? *Quarterly Journal of the Royal Meteorological Society*, *143*(709), 3025–3036. doi: 10.1002/qj

.3158

Butler, A. H., Sjoberg, J. P., Seidel, D. J., & Rosenlof, K. H. (2017). A sudden stratospheric warming compendium. *Earth System Science Data*, *9*(1), 63–76. doi: 10.5194/essd-9-63-2017

Cassou, C. (2008). Intraseasonal interaction between the Madden-Julian Oscillation and the North Atlantic Oscillation. *Nature*, *455*(7212), 523–527. doi: 10.1038/nature07286

Charlton, A. J., & Polvani, L. M. (2007). A new look at stratospheric sudden warmings. Part I: climatology and modelling benchmarks. *Journal of Climate*, *20*(3), 449–469. doi: 10.1175/JCLI3996.1

Charlton-Perez, A. J., Ferranti, L., & Lee, R. W. (2018). The influence of the stratospheric state on North Atlantic weather regimes. *Quarterly Journal of the Royal Meteorological Society*, *144*(713), 1140–1151. doi: 10.1002/qj.3280

Dee, D. P., Uppala, S. M., Simmons, A. J., Berrisford, P., Poli, P., Kobayashi, S., ... Vitart, F. (2011). The ERA-Interim reanalysis: configuration and performance of the data assimilation system. *Quarterly Journal of the Royal Meteorological Society*, *137*(656), 553–597. doi: 10.1002/qj.828

Ferranti, L., Magnusson, L., Vitart, F., & Richardson, D. S. (2018). How far in advance can we predict changes in large-scale flow leading to severe cold conditions over Europe? *Quarterly Journal of the Royal Meteorological Society*, *144*(715), 1788–1802. doi: 10.1002/qj.3341

Grams, C. M., Beerli, R., Pfenninger, S., Staffell, I., & Wernli, H. (2017). Balancing Europe's wind-power output through spatial deployment informed by weather regimes. *Nature Climate Change*, *7*(8), 557–562. doi: 10.1038/NCLIMATE3338

Hartmann, D. L. (2015). Pacific sea surface temperature and the winter of 2014. *Geophysical Research Letters*, *42*(6), 1894–1902. doi: 10.1002/2015GL063083

Karpechko, A. Y., Hitchcock, P., Peters, D. H. W., & Schneidereit, A. (2017). Predictability of downward propagation of major sudden stratospheric warmings. *Quarterly Journal of the Royal Meteorological Society*, *143*(704), 1459–1470. doi: 10.1002/qj.3017

Kidston, J., Scaife, A. A., Hardiman, S. C., Mitchell, D. M., Butchart, N., Baldwin, M. P., & Gray, L. J. (2015). Stratospheric influence on tropospheric jet streams, storm tracks and surface weather. *Nature Geoscience*, *8*(6), 433–440. doi: 10.1038/NGEO2424

Kodera, K., & Chiba, M. (1995). Tropospheric circulation changes associated with stratospheric sudden warmings: A case study. *Journal of Geophysical Research*, *100*(D6), 11055. doi: 10.1029/95JD00771

Kodera, K., Mukougawa, H., Maury, P., Ueda, M., & Claud, C. (2016). Absorbing and reflecting sudden stratospheric warming events and their relationship with tropospheric circulation. *Journal of Geophysical Research: Atmospheres*, *121*(1), 80–94. doi: 10.1002/2015JD023359

Kolstad, E. W., Breiteig, T., & Scaife, A. A. (2010). The association between stratospheric weak polar vortex events and cold air outbreaks in the Northern Hemisphere. *Quarterly Journal of the Royal Meteorological Society*, *136*(649), 886–893. doi: 10.1002/qj.620

Kretschmer, M., Cohen, J., Matthias, V., Runge, J., & Coumou, D. (2018). The different stratospheric influence on cold-extremes in Eurasia and North America. *npj Climate and Atmospheric Science*, *1*(1), 44. doi: 10.1038/s41612-018-0054-4

Limpasuvan, V., Hartmann, D. L., Thompson, D. W., Jeev, K., & Yung, Y. L. (2005). Stratosphere-troposphere evolution during polar vortex intensification. *Journal of Geophysical Research*, *110*(24), 1–15. doi: 10.1029/2005JD006302

Linkin, M. E., & Nigam, S. (2008). The North Pacific Oscillation-West Pacific teleconnection pattern: Mature-phase structure and winter impacts. *Journal of Climate*, *21*(9), 1979–1997. doi: 10.1175/2007JCLI2048.1

Michel, C., & Rivière, G. (2011). The Link between Rossby wave breakings and weather regime transitions. *Journal of the Atmospheric Sciences*, *68*(8), 1730–1748. doi: 10.1175/2011jas3635.1

Michelangeli, P.-A., Vautard, R., & Legras, B. (1995). Weather regimes: Recurrence and quasi stationarity. *Journal of the Atmospheric Sciences*, *52*(8), 1237–1256. doi: 10.1175/1520-0469(1995)052⟨1237:wrraqs⟩2.0.co;2

Mo, K. C., & Livezey, R. E. (1986). Tropical-extratropical geopotential height teleconnections during the Northern Hemisphere winter. *Monthly Weather Review*, *114*(12), 2488–2515. doi: 10.1175/1520-0493(1986)114⟨2488:teghtd⟩2.0.co;2

NOAA. (2019). *NOAA National Centers for Environmental Information (NCEI) U.S. Billion-Dollar Weather and Climate Disasters.* Retrieved 2019-08-01, from `https://www.ncdc.noaa.gov/billions/`

Pedregosa, F., Varoquaux, G., Gramfort, A., Michel, V., Thirion, B., Grisel, O., ... Duchesnay, E. (2011). Scikit-learn: Machine learning in Python. *Journal of Machine Learning Research*, *12*, 2825–2830.

Riddle, E. E., Stoner, M. B., Johnson, N. C., L'Heureux, M. L., Collins, D. C., & Feldstein, S. B. (2013). The impact of the MJO on clusters of wintertime circulation anomalies over the North American region. *Climate Dynamics*, *40*(7-8), 1749–1766. doi: 10.1007/s00382-012-1493-y

Robertson, A. W., & Ghil, M. (1999). Large-scale weather regimes and local climate over the western United States. *Journal of Climate*, *12*(6), 1796–1813. doi: 10.1175/1520-0442(1999)012⟨1796:LSWRAL⟩2.0.CO;2

Rogers, J. C. (1981). The North Pacific oscillation. *Journal of Climatology*, *1*(1), 39–57. doi: 10.1002/joc.3370010106

Sigmond, M., Scinocca, J. F., Kharin, V. V., & Shepherd, T. G. (2013). Enhanced seasonal forecast skill following stratospheric sudden warmings. *Nature Geoscience*, *6*(2), 98–102. doi: 10.1038/ngeo1698

Straus, D. M., Corti, S., & Molteni, F. (2007). Circulation regimes: Chaotic variability versus SST-forced predictability. *Journal of Climate*, *20*(10), 2251–2272. doi: 10.1175/JCLI4070.1

Thompson, D. W., & Wallace, J. M. (2001). Regional climate impacts of the Northern Hemisphere annular mode. *Science*, *293*, 85–89. doi: 10.1126/science.1058958

Tripathi, O. P., Baldwin, M., Charlton-Perez, A., Charron, M., Eckermann, S. D., Gerber, E., ... Son, S. W. (2015a). The predictability of the extratropical stratosphere on monthly time-scales and its impact on the skill of tropospheric forecasts. *Quarterly Journal of the Royal Meteorological Society*, *141*(689), 987–1003. doi: 10.1002/qj.2432

Tripathi, O. P., Charlton-Perez, A., Sigmond, M., & Vitart, F. (2015b). Enhanced long-range forecast skill in boreal winter following stratospheric strong vortex conditions. *Environmental Research Letters*, *10*(10), 104007. doi: 10.1088/1748-9326/10/10/104007

Vigaud, N., Robertson, A., & Tippett, M. (2018). Predictability of recurrent weather regimes over North America during winter from submonthly reforecasts. *Monthly Weather Review*, *146*(8), 2559–2577. doi: 10.1175/mwr-d-18-0058.1

Wang, S. Y. S., Huang, W. R., & Yoon, J. H. (2015). The North American winter 'dipole' and extremes activity: A CMIP5 assessment. *Atmospheric Science Letters*, *16*(3), 338–345. doi: 10.1002/asl2.565

Waugh, D. W., Sobel, A. H., & Polvani, L. M. (2017). What is the polar vortex and how does it influence weather? *Bulletin of the American Meteorological Society*, *98*(1), 37–44. doi: 10.1175/BAMS-D-15-00212.1

Wilks, D. (2011). *Statistical methods in the atmospheric sciences.* Academic Press.

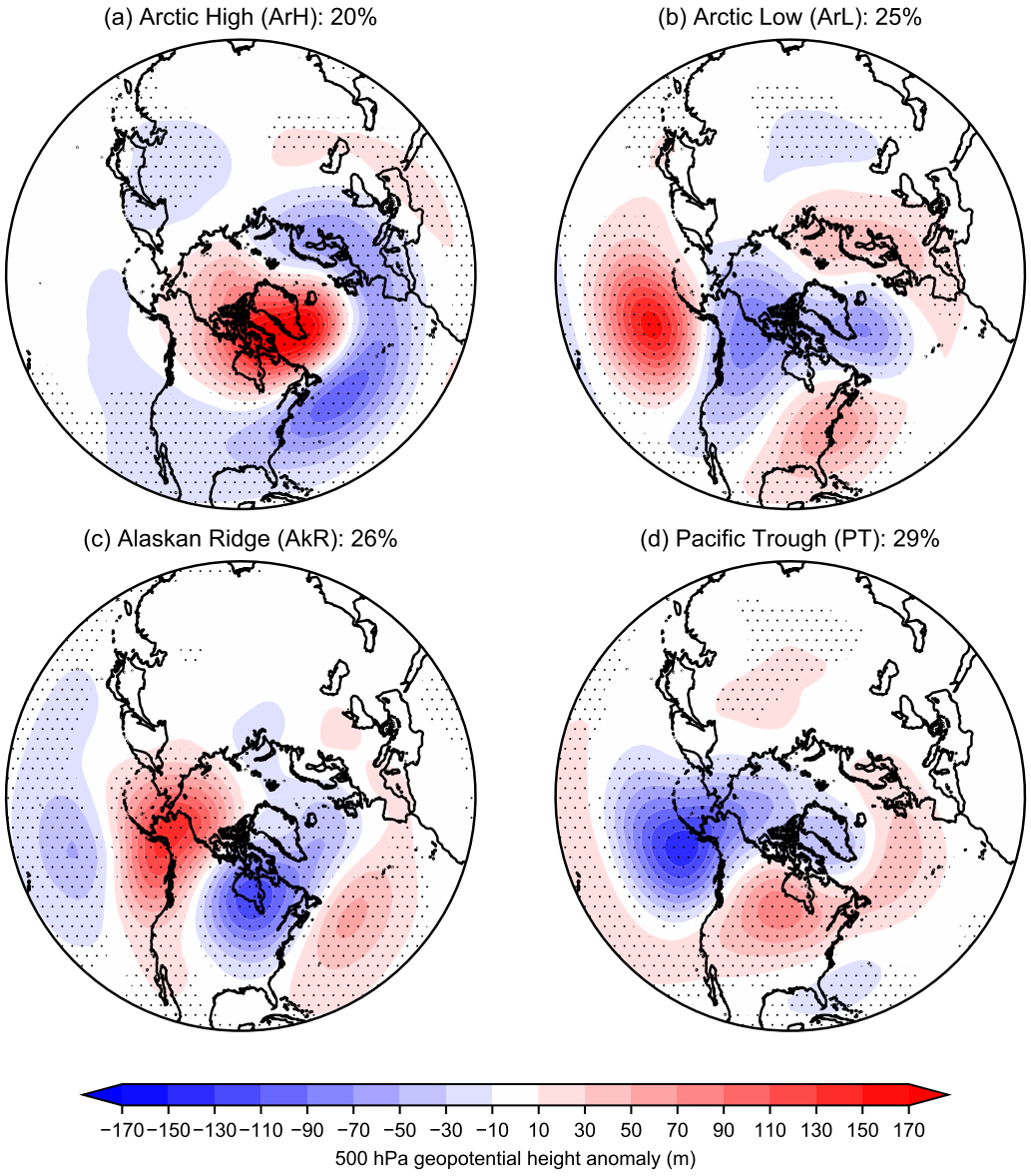

Figure 1. Composite mean 500 hPa geopotential height anomalies (meters) for each of the four regimes. Anomalies are expressed with respect to the de-trended daily January 1979–December 2017 mean. Percentages indicate the occupation frequency of the regime (the percentage of days assigned to the regime in the November–March period). Stippling indicates significance at the 95% confidence level according to a two-sided bootstrap re-sampling test.

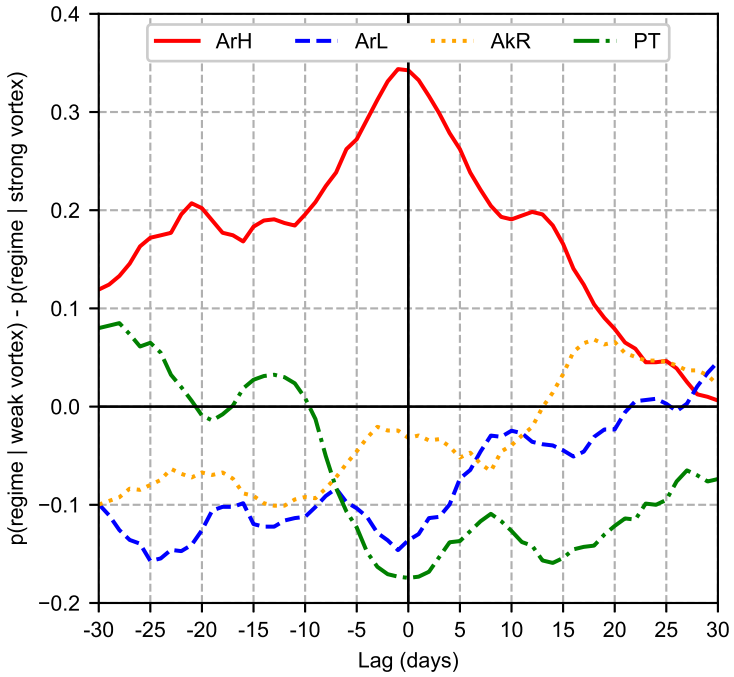

Figure 2. Difference in the occurrence probability of each regime between weak and strong stratospheric polar vortex states for -30 to +30 day lags, conditional on the vortex state at day 0.

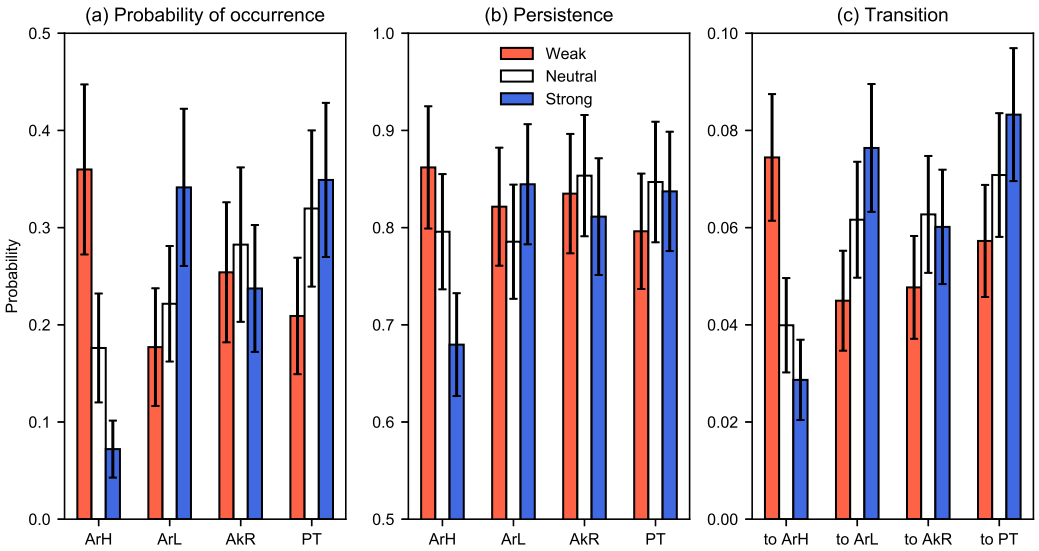

Figure 3. (a) Probability of occurrence, (b) persistence, and (c) transition of each regime given the tercile category of the stratospheric polar vortex strength on the preceding day. Error bars indicate 95% binomial proportion confidence intervals using a normal approximation (see text for details). Colors indicate the tercile category of the 100 hPa 60°N zonal-mean zonal wind based on daily January 1979–December 2017 climatology.

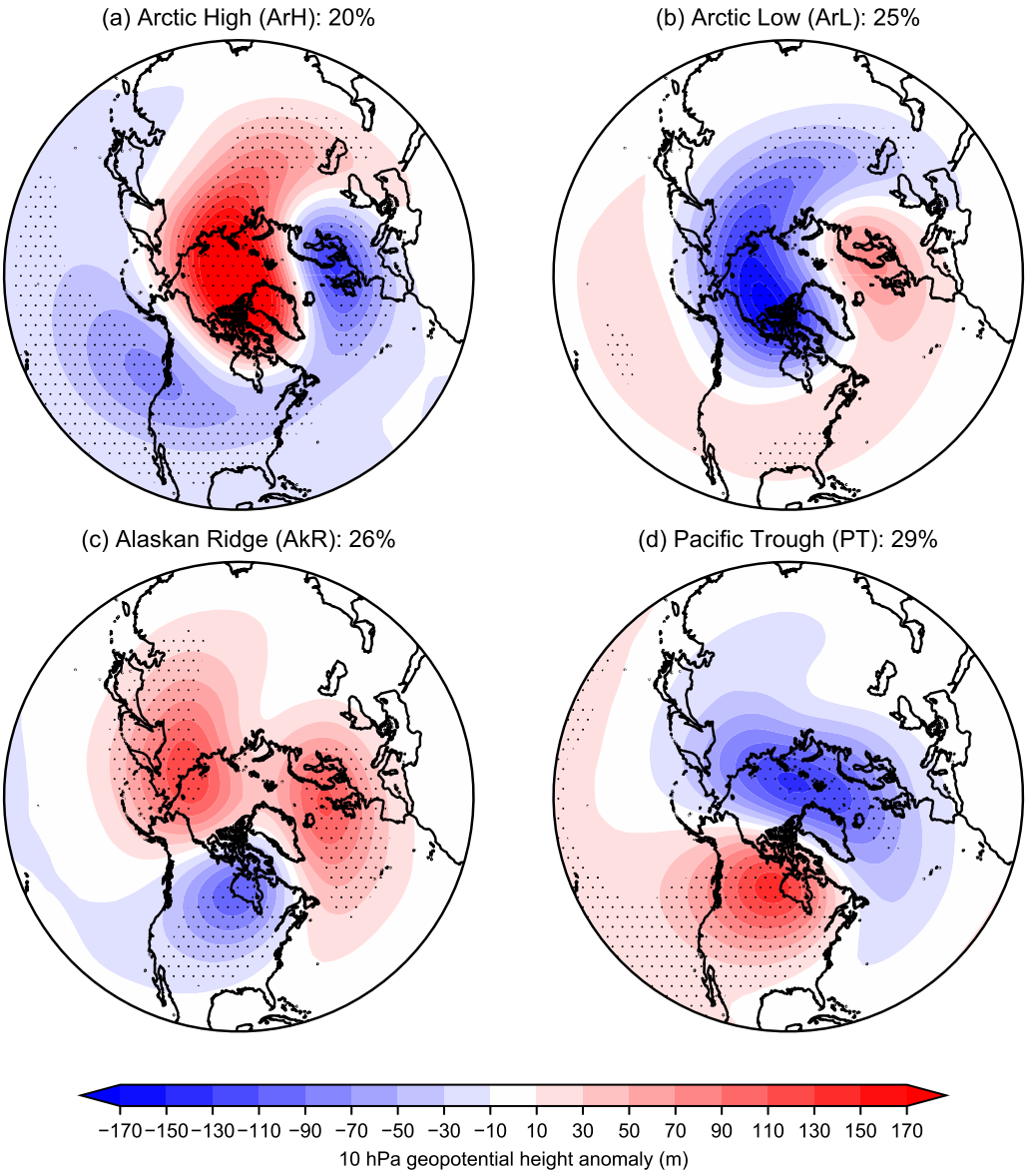

Figure 4. Composite mean 10 hPa geopotential height anomalies (meters) for days classified in each of the four regimes. Anomalies are expressed with respect to the de-trended January 1979–December 2017 mean. Stippling indicates significance at the 95% confidence level according to a two-sided bootstrap re-sampling test.

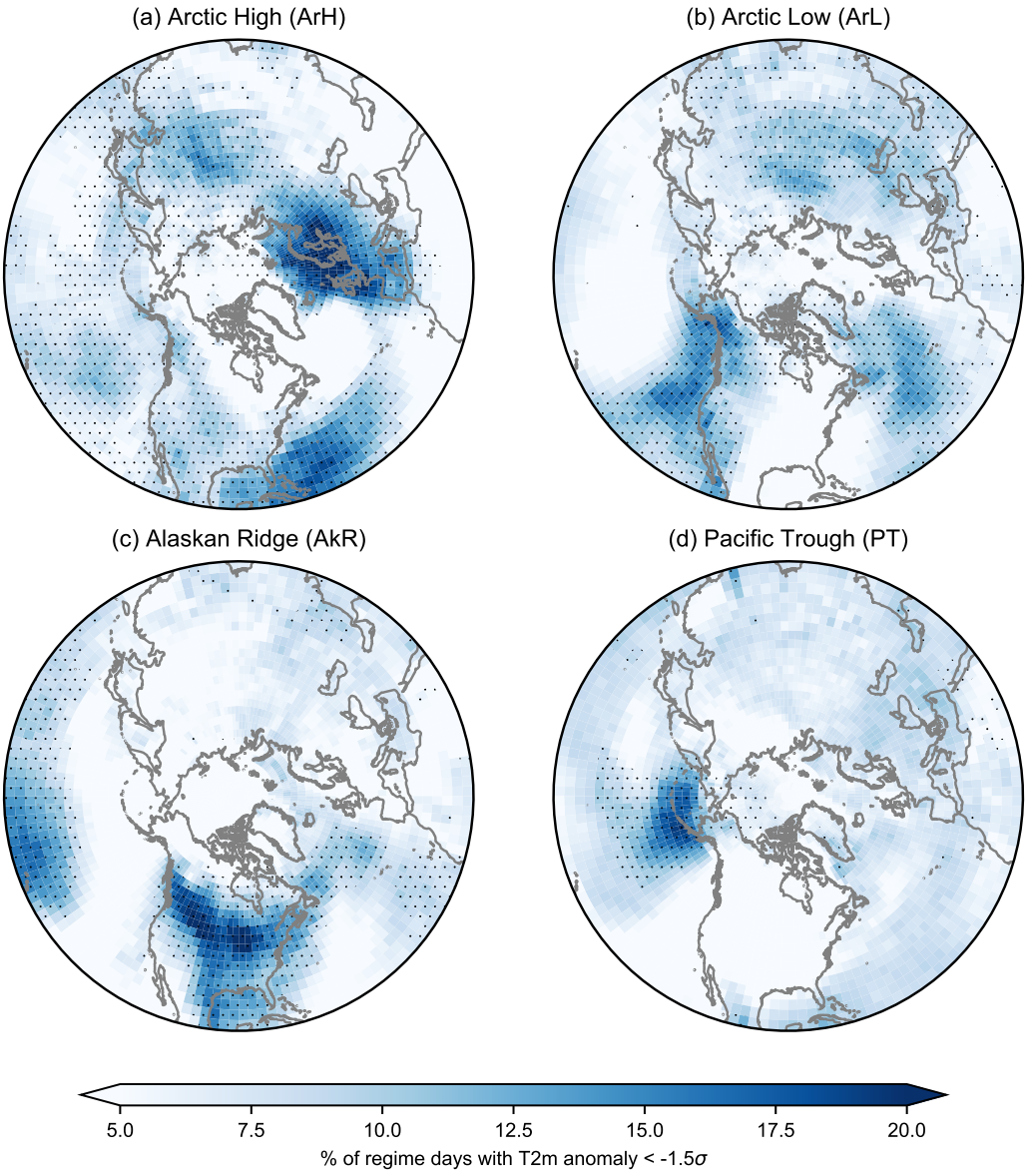

Figure 5. Percent of all days in each regime with daily standardized 2 m temperature anomalies < -1.5 σ (with respect to the linearly de-trended daily January 1979–December 2017 mean). Stippling indicates significance at the 95% confidence level according to a one-sided bootstrap re-sampling test.